AIAA Aviation
16-20 June 2014, Atlanta, GA
AIAA Atmospheric Flight Mechanics Conference

Extension and Enhancement of the Allen-Eggers Analytic Solution for Ballistic Entry Trajectories

Zachary R. Putnam* and Robert D. Braun†
Georgia Institute of Technology, Atlanta, Georgia, 30332

The closed-form analytic solution to the equations of motion for ballistic entry developed by Allen and Eggers is extended and enhanced with a method of choosing an appropriate constant flight-path angle, limits based on the equations of motion and acceptable approximation error are proposed that bound the domain of applicability, and closed-form expressions for range and time-dependency. The expression developed for range to go exhibits error that may low enough for onboard drag-modulation guidance and targeting systems. These improvements address key weaknesses in the original approximate solution. Results show that the extended and enhanced Allen-Eggers solution provides good accuracy across a range of ballistic coefficients entries at Earth with initial flight-path angles steeper than -7 deg.

Nomenclature

A	=	aerodynamic reference area, m^2
a	=	acceleration magnitude, Earth g
C_D	=	drag coefficient
C_L	=	lift coefficient
D	=	qAC_D, drag magnitude, N
E	=	energy over weight, m
g	=	acceleration due to gravity, m/s^2
H	=	atmospheric scale height, m
h	=	altitude, m
k	=	convective stagnation-point heat rate constant, $kg^{1/2}m^{-1}$
L	=	qAC_L, lift magnitude, N
L/D	=	lift-to-drag ratio
m	=	mass, kg
q	=	$(1/2)\rho V^2$, dynamic pressure, N/m^2
$\dot{Q}$	=	convective stagnation-point heat rate, W/cm^2
R	=	planetary radius, m
r_n	=	effective nose radius, m
S	=	range, m
S_{togo}	=	range to go, m
t	=	time, s
V	=	velocity magnitude, m/s
V_C	=	circular velocity, m/s
W	=	mg, weight magnitude, N
$\bar{\gamma}$	=	Euler's constant
β	=	$m/(C_D A)$, ballistic coefficient, kg/m^2
δ_q	=	initial dynamic pressure stand-off factor
δ_V	=	final velocity stand-off factor

*Graduate Research Assistant, School of Aerospace Engineering, 270 Ferst Dr., Senior Member AIAA.
†Professor, School of Aerospace Engineering, 270 Ferst Dr., Fellow AIAA

γ = flight-path angle, positive above local horizontal, rad
γ^* = Allen-Eggers constant flight-path angle, rad
ρ = atmospheric density, kg/m^3
θ = range angle, rad

I. Introduction

When planetary entry was first studied in the middle of the twentieth century, analytic approximations were developed to enable vehicle and mission designers to evaluate vehicle trajectories and performance with minimal or no computer usage. Seminal examples of these approximations include, in chronological order, Sänger's expressions for lifting entry,[1] the Allen-Eggers approximation for ballistic entry,[2] Chapman's Z-function,[3] Loh's "second-order" approximation,[4] and those developed by Vinh et al.[5] These analytic and hybrid analytic-numeric approximate solutions utilized assumptions to make the nonlinear equations of motion soluble. As a result, they typically only applied to limited classes of entry vehicles and trajectories.

Advances in computing eventually made high-accuracy numeric integration of the equations of motion feasible for most applications.[6] Today, vehicle and mission designers have significant computational resources available, enabling relatively rapid, low-cost, and high-fidelity assessment of entry trajectories. However, approximate solutions are still desirable for some applications when simplicity and execution speed are paramount, such as real-time guidance, navigation, and control systems; optimization; and conceptual design. Analytic solutions also provide more information about classes of trajectories: they may be manipulated to determine parameter sensitivities and partial derivatives. It is with these applications in mind that this study seeks to extend and enhance the Allen-Eggers approximate solution for ballistic entry through development of a method for computing the assumed constant flight-path angle, bounds for the domain of applicability, and closed-form expressions for trajectory range and time.

Harry "Harvey" Julian Allen and Alfred J. Eggers, working at the Ames Aeronautical Laboratory, first documented their approximate solution for ballistic (nonlifting) entry in a classified NACA research memorandum in 1953.[7] This memorandum was declassified in 1957,[7] and subsequently republished as a NACA report in 1958.[2] The primary goal of Allen's and Eggers' work was "to determine means available to the designer for minimizing aerodynamic heating" for missile applications.[2] The Allen-Eggers approximate solution is based on the insight that, for ballistic entry at a sufficiently steep initial flight-path angle, the gravitational force may be neglected because its magnitude is small relative to the magnitude of the drag force.[2] This yields a closed-form analytic relationship between velocity and altitude from which Allen and Eggers were able to derive closed-form analytic expressions for deceleration and heating, including state values at peak conditions of interest. The solution is composed of relatively simple, explicit analytic expressions.

II. Methods and Assumptions

A. Planar Equations of Motion

The hypersonic phase of planetary entry is typically unpowered; thrust is used only for attitude control, if at all. The small amount of thrust required for attitude control results in a nearly constant vehicle mass. The scalar, planar equations of motion may be derived by considering the coordinate systems and free-body diagram for a planar entry trajectory shown in Fig. 1.[8] The coordinate frames are the inertial frame (X^I, Z^I), the local horizontal frame (X^L, Z^L), and the wind frame (X^W, Z^W). Expressing the vectors in Fig. 1 in the wind frame, one can use Newton's second law to write two scalar equations of motion:

$$\frac{dV}{dt} = -\frac{D}{m} - \frac{W}{g}\sin(\gamma) \tag{1a}$$

$$\frac{d\gamma}{dt} = \frac{d\theta}{dt} + \frac{1}{V}\frac{L}{m} - \frac{W}{gV}\cos(\gamma) \tag{1b}$$

From kinematics, two more equations may be written for altitude above the planetary surface and range angle, assuming a spherical planetary surface:

$$\frac{dh}{dt} = V \sin\gamma \tag{2a}$$

$$\frac{d\theta}{dt} = \frac{V\cos(\gamma)}{h+R} \tag{2b}$$

The acceleration due to gravity changes little during entry, as altitude changes are one to two orders of magnitude less than planetary radii for most applications. Therefore, g is assumed to be constant during entry. Atmospheric density is assumed to vary exponentially with altitude according to:

$$\rho = \rho_{ref} \exp\left(\frac{h_{ref} - h}{H}\right) \tag{3}$$

While the scale height varies with altitude in a real atmosphere, the most interesting aspects of planetary entry, such as peak deceleration and peak heating, occur in a relatively narrow altitude band, making the assumption of constant scale height reasonable with appropriate selection of ρ_{ref} and h_{ref}. The reference density need not be selected as the zero-altitude density; choosing ρ_{ref} and H associated with a higher altitude may produce a more accurate representation of the true atmospheric density profile over the altitude range of interest.

The equations of motion can be simplified by assuming constant values for the aerodynamic coefficients and thus for β and L/D. While the aerodynamic properties of an entry vehicle generally vary with Mach number and angle-of-attack to first order, Mach-number independence in the hypersonic flight regime (Mach numbers above about 5) makes constant aerodynamic coefficients a good assumption for most planetary entry trajectories.[9]

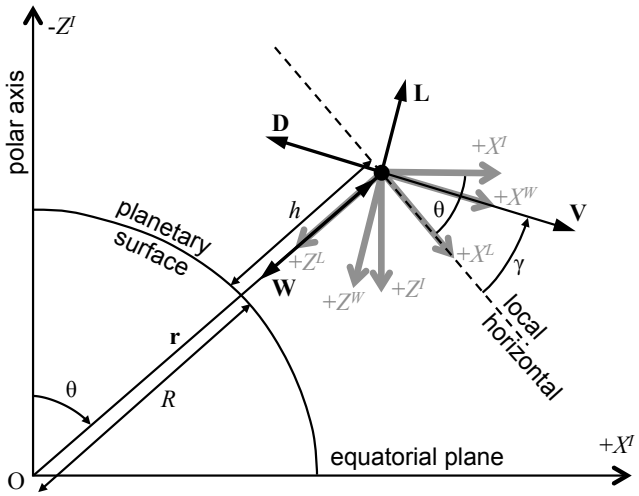

Figure 1. Coordinate systems and free-body diagram for a planar planetary entry trajectory.

Combining Eqs. (1) through (3) and rearranging terms, the planar equations of motion for a planetary entry vehicle may be written as:

$$\frac{dV}{dt} = -\left[\frac{\rho_{ref}}{2\beta}\exp\left(\frac{h_{ref}-h}{H}\right)\right]V^2 - g\sin(\gamma) \tag{4a}$$

$$\frac{d\gamma}{dt} = \frac{V\cos\gamma}{R+h} + \left[\frac{\rho_{ref}}{2\beta}\exp\left(\frac{h_{ref}-h}{H}\right)\right]\left(\frac{L}{D}\right)V - \frac{g}{V}\cos(\gamma) \tag{4b}$$

$$\frac{dh}{dt} = V\sin(\gamma) \tag{4c}$$

$$\frac{d\theta}{dt} = \frac{V\cos\gamma}{R+h} \tag{4d}$$

Eqs. (4) are a set of coupled, first-order, ordinary differential equations. These equations are highly nonlinear due to the presence of the planetary atmosphere and defy analytic solution unless simplifying assumptions are applied.

B. Computational Methods

In this study, approximation errors generally are presented as a percentage relative to Eqs. (4). Eqs. (4) are solved numerically using Matlab's intrinsic ode45 function with absolute and relative error tolerances of 10^{-12}. Error presented as absolute error is the absolute value of the error magnitude. The normalized integrated error is used to compare approximation error across multiple trajectories and is defined by:

$$\varepsilon_X = \frac{1}{\varepsilon_{X,norm}} \sqrt{\sum_{i=1}^{N} \left(\frac{X_{i,approx} - X_{i,EOM}}{X_{i,EOM}} \right)^2} \tag{5}$$

where N is the total number of points computed for the trajectory and X represents the trajectory state of interest. While individual values of this integrated error are physically meaningless, they provide an estimate of the efficacy of an approximate solution relative to a known trajectory. The Mathematica computer algebra system was used to symbolically evaluate the complex integrals in this study.

C. Example Entry Trajectories

Three example trajectories were chosen to illustrate the extension and enhancement of the Allen-Eggers approximate solution: interplanetary robotic sample return, strategic reentry, and low-Earth orbit (LEO) return of crew from the International Space Station. These example trajectories span a range of initial conditions and vehicle parameters and represent current ballistic entry missions of interest at Earth to the entry community (see Table 1). The sample-return example is based on NASA's Stardust Sample Return Capsule, which successfully landed after a ballistic entry in 2006.[10] Stardust had the greatest initial velocity of any Earth-return mission. The strategic example features a high ballistic coefficient vehicle on a steep, high-energy suborbital trajectory.[11] The LEO-return example represents ballistic entry of a crewed vehicle and is based on data from the off-nominal ballistic entry of Soyuz TMA-11.[13] This example is consistent with other blunt-body crewed entry systems and enters the atmosphere at a very shallow flight-path angle. Together, these examples include hyperbolic, orbital, and suborbital entry energies and span several orders of magnitude of ballistic coefficient.

Table 1. Parameters for Example Trajectories at Earth

Parameter	Sample Return[10, 12]	Strategic[11]	LEO Return[13]
Equatorial radius, R	6378.0 km	6378.0 km	6378.0 km
Gravitational acceleration, g	9.81 m/s^2	9.81 m/s^2	9.81 m/s^2
Atmospheric scale height, H	8.5 km	8.5 km	8.5 km
Reference atmospheric density, ρ_{ref}	1.215 kg/m^3	1.215 kg/m^3	1.215 kg/m^3
Reference altitude, h_{ref}	0 km	0 km	0 km
Initial velocity, V_0	12.8 km/s	7.2 km/s	7.9 km/s
Initial flight-path angle, γ_0	-8.2 deg	-30.0 deg	-1.35 deg
Initial altitude, h_0	125 km	125 km	100 km
Ballistic coefficient, β	60 kg/m^2	10000 kg/m^2	450 kg/m^2
Lift-to-drag ratio, L/D	0	0	0

III. Review and Modernization of the Allen-Eggers Solution

The Allen-Eggers solution is rederived below using modern nomenclature. The results differ slightly from those presented in Ref. 2 due to use of the current convention for the definition of flight-path angle and ballistic coefficient. A more general atmosphere model including a reference altitude is also used.

A. Altitude-Velocity Profile

The Allen-Eggers altitude-velocity profile may be derived by recognizing that for sufficiently steep entries the drag force magnitude is much greater than the gravity force magnitude. Eqs. (4) are well-suited for modeling ballistic entry, because ballistic vehicles have no out-of-plane control authority. Starting from Eq. (4a) and neglecting the gravity term relative to the drag term, one may write:

$$\frac{dV}{dt} = -\frac{\rho_{ref}}{2\beta} \exp\left(\frac{h_{ref} - h}{H}\right) V^2 \tag{6}$$

Rearranging Eq. (4c) yields:

$$V = \frac{1}{\sin\gamma} \frac{dh}{dt} \tag{7}$$

Substituting Eq. (7) into Eq. (6) and separating variables gives:

$$\frac{1}{V}\frac{dV}{dt} = -\frac{\rho_{ref}}{2\beta \sin\gamma} \exp\left(\frac{h_{ref} - h}{H}\right) \frac{dh}{dt} \tag{8}$$

Assuming a constant flight-path angle γ^* and eliminating dt, this expression can be integrated from some state 1 to some state 2 and solved for V_2:

$$V_2 = V_1 \exp\left\{\frac{H\rho_{ref}}{2\beta \sin\gamma^*}\left[\exp\left(\frac{h_{ref} - h_2}{H}\right) - \exp\left(\frac{h_{ref} - h_1}{H}\right)\right]\right\} \tag{9}$$

This expression, first derived by Allen and Eggers, determines an altitude-velocity profile (h_2, V_2) as a function of the planetary atmosphere (ρ_{ref}, h_{ref}, H), vehicle properties (β), and a reference vehicle state $(V_1, h_1, \gamma_1 = \gamma^*)$. Allen and Eggers suggest using the initial flight-path angle for γ^*;[2] this approach works well for the steep entry trajectories ($\gamma_0 \ll 0$) that were of interest to Allen and Eggers. Lastly, Eq. (9) assumes that velocity is monotonically decreasing with altitude, limiting application of this approximate solution to trajectories with no positive altitude rate.

B. Acceleration Magnitude

Combining Eqs. (6) and (9) results in an equation for the acceleration magnitude. This expression, normalized by g, is given by:

$$a_2 = -\left.\frac{dV/dt}{g}\right|_2 = \frac{\rho_{ref}}{2\beta g} V_1^2 \exp\left(\frac{h_{ref} - h_2}{H}\right) \exp\left\{\frac{H\rho_{ref}}{\beta \sin\gamma^*}\left[\exp\left(\frac{h_{ref} - h_2}{H}\right) - \exp\left(\frac{h_{ref} - h_1}{H}\right)\right]\right\} \tag{10}$$

Eq. (10) yields a relatively simple expression for the altitude at peak deceleration:

$$h_{a_{max}} = h_{ref} + H \ln\left(-\frac{H\rho_{ref}}{\beta \sin\gamma^*}\right) \tag{11}$$

Combining Eq. (11) and Eq. (9), the velocity at peak deceleration is:

$$V_{a_{max}} = \frac{V_1}{\sqrt{e}} \exp\left[-\frac{H\rho_{ref}}{2\beta \sin\gamma^*} \exp\left(\frac{h_{ref} - h_1}{H}\right)\right] \tag{12}$$

The maximum acceleration is given by:

$$a_{max} = -\frac{\sin\gamma^*}{2egH} V_1^2 \exp\left[-\frac{H\rho_{ref}}{\beta \sin\gamma^*} \exp\left(\frac{h_{ref} - h_1}{H}\right)\right] \tag{13}$$

If $h_{a_{max}}$ is below the planetary surface, peak deceleration occurs at minimum altitude h_{min} and is given by:

$$a_{max} = \frac{\rho_{ref}}{2\beta g} V_1^2 \exp\left(\frac{h_{ref} - h_{min}}{H}\right) \exp\left\{\frac{H\rho_{ref}}{\beta \sin\gamma^*}\left[\exp\left(\frac{h_{ref} - h_{min}}{H}\right) - \exp\left(\frac{h_{ref} - h_1}{H}\right)\right]\right\} \tag{14}$$

where the velocity is:

$$V_{a_{max}} = V_1 \exp\left\{\frac{H\rho_{ref}}{2\beta \sin\gamma^*}\left[\exp\left(\frac{h_{ref} - h_{min}}{H}\right) - \exp\left(\frac{h_{ref} - h_1}{H}\right)\right]\right\} \tag{15}$$

C. Convective Heat Rate

Allen and Eggers formulated an equation for the convective heat rate at the stagnation point of a blunt-body vehicle:[2]

$$\dot{Q} = k\sqrt{\frac{\rho}{r_n}}V^3 \tag{16}$$

This equation assumes that the vehicle is sufficiently blunt such that a detached bow shock exists ahead of the body. Blunt leading edges for hypersonic vehicles are an innovation developed by Allen as a way to reduce the severity of entry heating on the vehicle.[14] In Allen's and Eggers' original document, k is given a value of 6.8×10^{-6} without units;[2] dimensional analysis indicates k has units of $\mathrm{kg}^{1/2}\mathrm{m}^{-1}$. A value for k suitable for application at Earth was computed using the method developed by Sutton and Graves.[15]

Combining Eq. (16) and Eq. (9) results in an expression for heat rate as a function of altitude:

$$\dot{Q}_2 = k\sqrt{\frac{\rho_{ref}}{r_n}}V_1^3 \exp\left(\frac{h_{ref}-h_2}{2H}\right)\exp\left\{\frac{3H\rho_{ref}}{2\beta\sin\gamma^*}\left[\exp\left(\frac{h_{ref}-h_2}{H}\right)-\exp\left(\frac{h_{ref}-h_1}{H}\right)\right]\right\} \tag{17}$$

The altitude and velocity at maximum heat rate are given by:

$$h_{\dot{Q}_{max}} = h_{ref} + H\ln\left(-\frac{3H\rho_{ref}}{\beta\sin\gamma^*}\right) \tag{18}$$

$$V_{\dot{Q}_{max}} = \frac{V_1}{e^{1/6}}\exp\left[-\frac{H\rho_{ref}}{2\beta\sin\gamma^*}\exp\left(\frac{h_{ref}-h_1}{H}\right)\right] \tag{19}$$

The maximum heat rate is (for $h_{\dot{Q}_{max}} \geq h_{min}$):

$$\dot{Q}_{max} = k\sqrt{-\frac{\beta\sin\gamma^*}{3eHr_n}}V_1^3\exp\left[-\frac{3H\rho_{ref}}{2\beta\sin\gamma^*}\exp\left(\frac{h_{ref}-h_1}{H}\right)\right] \tag{20}$$

Otherwise, the maximum heat rate occurs at the minimum altitude ($h = h_{min}$) and the peak heat rate is given by:

$$\dot{Q}_{max} = k\sqrt{\frac{\rho_{ref}}{r_n}}V_1^3\exp\left(\frac{h_{ref}-h_{min}}{2H}\right)\exp\left\{\frac{3H\rho_{ref}}{2\beta\sin\gamma^*}\left[\exp\left(\frac{h_{ref}-h_{min}}{H}\right)-\exp\left(\frac{h_{ref}-h_1}{H}\right)\right]\right\} \tag{21}$$

The velocity at this condition is given by Eq. (15).

D. Simplified Expressions

Setting h_{ref} to 0 m, state 2 to the current state (without subscript), and state 1 to the initial vehicle state near the top of the atmosphere (designated by the subscript 0) such that $\exp[-h/H] \gg \exp[-h_0/H]$, a simpler expression for the altitude-velocity profile results:

$$V = V_0\exp\left[\frac{H\rho_{ref}}{2\beta\sin\gamma^*}\exp\left(-\frac{h}{H}\right)\right] \tag{22}$$

where ρ_{ref} is now the density at zero altitude. These assumptions also simplify the expressions for acceleration and the conditions at maximum acceleration. Eq. (10) becomes:

$$a = \frac{\rho_{ref}}{2\beta g}V_0^2\exp\left(-\frac{h}{H}\right)\exp\left[\frac{H\rho_{ref}}{\beta\sin\gamma^*}\exp\left(-\frac{h}{H}\right)\right] \tag{23}$$

The conditions at peak acceleration are then given by (for $h_{a_{max}} > h_{min}$):

$$h_{a_{max}} = H\ln\left(-\frac{H\rho_{ref}}{\beta\sin\gamma^*}\right) \tag{24}$$

$$V_{a_{max}} = \frac{V_0}{\sqrt{e}} \approx (0.6065)V_0 \tag{25}$$

$$a_{max} = -\frac{\sin\gamma^*}{2egH} V_0^2 \tag{26}$$

The expression for heat rate becomes:

$$\dot{Q} = k\sqrt{\frac{\rho_{ref}}{r_n}} V_0^3 \exp\left(-\frac{h}{2H}\right) \exp\left[\frac{3H\rho_{ref}}{2\beta\sin\gamma^*} \exp\left(-\frac{h}{H}\right)\right] \tag{27}$$

The conditions at peak heat rate are then (for $h_{\dot{Q}_{max}} > h_{min}$):

$$h_{\dot{Q}_{max}} = H \ln\left(-\frac{3H\rho_{ref}}{\beta\sin\gamma^*}\right) \tag{28}$$

$$V_{\dot{Q}_{max}} = \frac{V_0}{e^{1/6}} \approx (0.8465)V_0 \tag{29}$$

$$\dot{Q}_{max} = k\sqrt{-\frac{\beta\sin\gamma^*}{3eHr_n}} V_0^3 \tag{30}$$

These simplified expressions are closer in form to those originally presented by Allen and Eggers.[2] They also provide insight into several phenomena. First, the altitudes at which maximum acceleration and heat rate occur are not functions of velocity: they are dictated entirely by vehicle parameters, planetary parameters, and the flight-path angle. In contrast, the velocities at maximum acceleration and heat rate are fractions of the initial velocity only, and peak heating always occurs prior to peak deceleration. Lastly, as one might expect, maximum acceleration and heat rate are driven primarily by the initial velocity of the vehicle: greater initial kinetic energies result in greater values of acceleration and heat rate.

E. Example Applications

Figure 2 shows example applications of the modernized Allen-Eggers approximate solution to the three planetary entry trajectories specified in Table 1. The approximate trajectories are co-plotted with numeric solutions to Eqs. (4). Error plots are provided in Fig. 3. The Allen-Eggers approximation shows good agreement with the planar equations of motion for the strategic case. The altitude (Fig. 2a) and heat-rate profiles (Fig. 2d) show small approximation errors for the sample-return case, but the acceleration error is nearly 50%. The Allen-Eggers solution does a poor job approximating the shallow LEO-return case.

The assumptions used in the derivation of the Allen-Eggers solution lead to the smallest error during the hypersonic portion of the trajectory. This regime encompasses the acceleration and heating pulses, including peak values for these quantities. These quantities and qualities of a planetary entry trajectory typically drive entry vehicle and mission design, making the Allen-Eggers approximate solution a useful tool for conceptual mission and vehicle design and analysis. Values of vehicle states at peak acceleration and peak heat rate estimated by the Allen-Eggers approximation are given in Tables 2 and 3, respectively. As before, errors for the strategic example are uniformly low. Estimates of conditions at peak heat rate are within 20% for both the sample-return and LEO-return cases; estimation error for peak acceleration is significantly larger for these cases. Reducing in this error will make Allen-Eggers approximation applicable for estimating states at peak conditions for more mission classes.

The nature of the error in Fig. 3 points towards several weaknesses in the solution. First, while choosing the initial flight-path angle appears to be a good choice for γ^* for the strategic case, this is not true for the other cases. Second, development of bounds on the domain of applicability on the solution would provide the user with greater confidence in the approximation without direct comparison with numeric solutions. Lastly, the Allen-Eggers solution does not provide any information on range or time of flight for entry, both of which are useful quantities for onboard guidance and targeting systems.

IV. Extensions and Enhancements to the Allen-Eggers Solution

Several extensions and enhancements to the Allen-Eggers approximate solution are proposed to address implementation weaknesses, provide additional information, and extend applicability of the solution: a method for computing the constant flight-path angle, bounds on the domain of applicability, closed-form

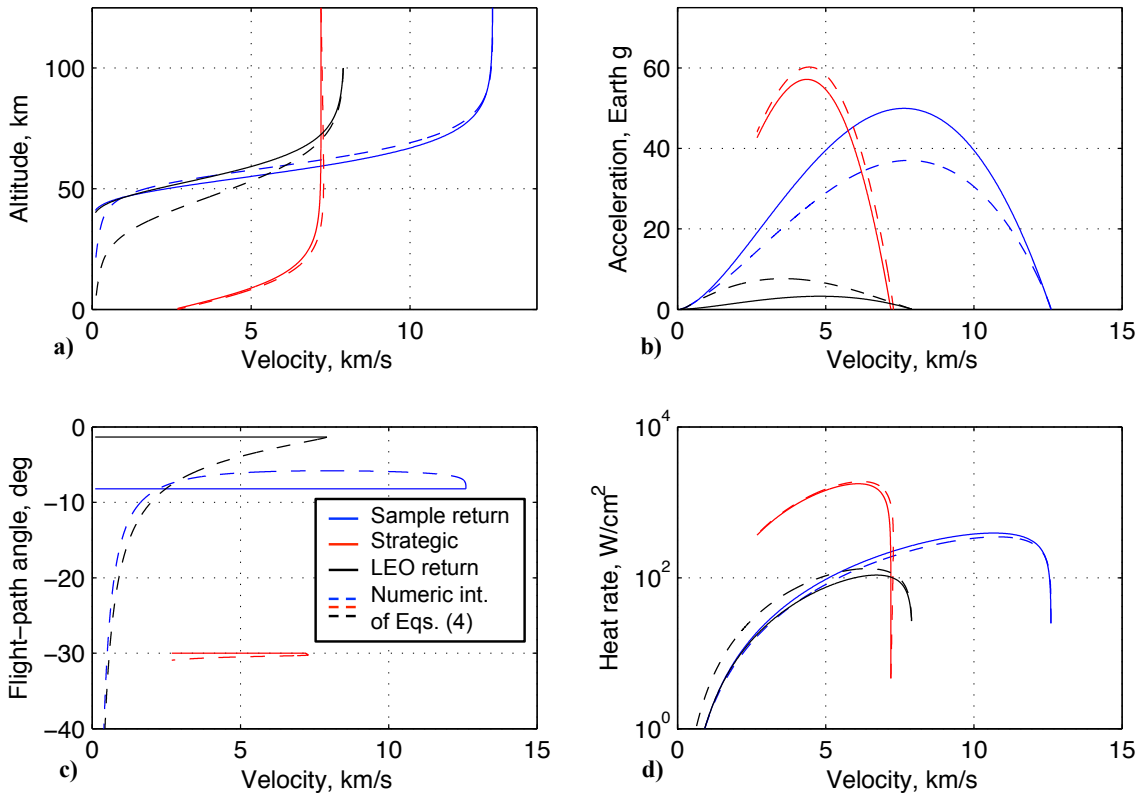

Figure 2. Example application of the Allen-Eggers approximate solution: a) altitude, b) acceleration, c) flight-path angle, and d) heat rate versus velocity.

Table 2. Vehicle States at Peak Acceleration

	Acceleration		Velocity		Altitude	
	Value, g	Error, %	Value, km/s	Error, %	Value, km	Error, %
Sample return	50.0	34.9	7.64	-2.1	60.3	-4.6
Strategic	57.2	-5.1	4.37	-1.8	6.2	3.6
LEO return	3.3	-57.3	4.81	34.9	58.5	27.0

Table 3. Vehicle States at Peak Heat Rate

	Heat rate		Velocity		Altitude	
	Value, W/cm^2	Error, %	Value, km/s	Error, %	Value, km	Error, %
Sample return	391.5	12.3	10.67	-1.2	69.7	-3.6
Strategic	1764.3	-6.5	6.09	-1.8	15.5	1.3
LEO return	108.5	-18.0	6.71	4.7	67.8	9.2

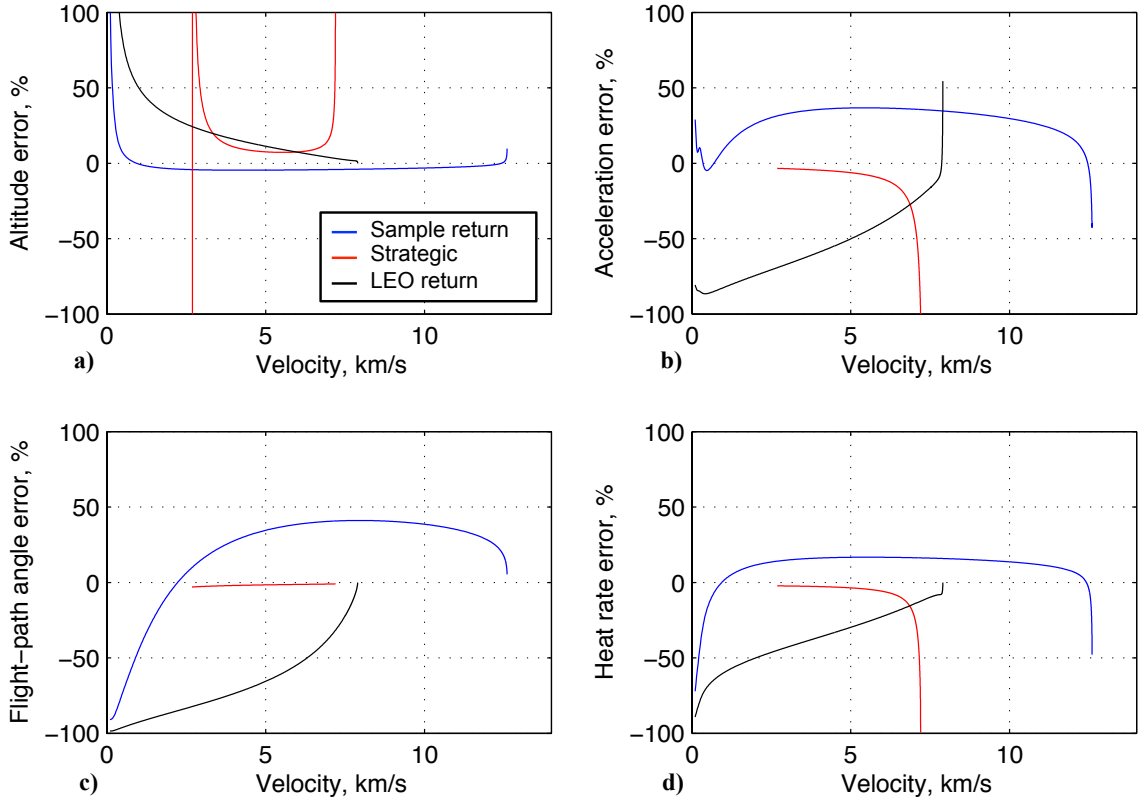

Figure 3. Allen-Eggers approximation error for a) altitude, b) acceleration, c) flight-path angle, and d) heat rate versus velocity.

expressions for range, and formulation of the approximation as a function of time. In an effort to maintain the character of the Allen-Eggers solution, these developments result in explicit, analytic, and relatively simple expressions.

A. Determining the Constant Flight-Path Angle

A singular issue when applying the Allen-Eggers approximate solution to a real-world problem is determining a proper value for γ^*, the assumed constant flight-path angle. Steep entries exhibit only a small change in flight-path angle from its initial value in the hypersonic regime, making γ_0 a good approximation of γ^*; shallow trajectories fly at near-constant flight-path angles that are significantly different from the initial value, making γ_0 a relatively poor choice for γ^*. The ability to accurately determine more appropriate values for γ^* will extend the domain of applicability of the Allen-Eggers approximate solution to more shallow initial flight-path angles and improve overall accuracy.

1. *Determining γ^**

It is desirable to develop a method for determining γ^* based on available information that that is closed-form, explicit, and does not require numeric integration to preserve the advantages of the Allen-Eggers solution. The solution for flight-path angle as a function of velocity developed by Citron and Meir meets these criteria.[16] Other approximate solutions for flight-path angle were considered: Loh's "Second-order" solution,[4] Yaroshevskiy's series approximation,[17,18] and Chapman's z-function solution.[3] However, none were explicit, analytic, and generally-applicable.

The Citron-Meir expression for flight-path angle is, rederived to be consistent with nomenclature defined in this study and with $L/D = 0$:

$$\sin\gamma = \sin\gamma_0\,(2F - 1) \tag{31}$$

where

$$F = \left[1 + \frac{H}{R\tan^2\gamma_0}\left\{\frac{V_C^2}{V_0^2}\left[\mathrm{Ei}\left(\ln\frac{V_0^2}{V^2}\right) - \bar{\gamma} - \ln\left(\ln\frac{V_0^2}{V^2}\right)\right] + \left(\frac{V_C^2}{V_0^2} - 1\right)\ln\left(1 - \frac{\beta\sin\gamma_0}{H\rho_0}\ln\frac{V_0^2}{V^2}\right)\right\}\right]^{1/2} \tag{31a}$$

where ρ_0 is the density at V_0 and Ei is the exponential integral, defined by:

$$\mathrm{Ei}(x) = -\int_{-x}^{\infty}\frac{\exp(-y)}{y}dy \tag{32}$$

The exponential integral may be approximated using the explicit, analytic method developed by Cody and Thacher.[19] Given an initial state, planetary properties, and ballistic coefficient, Eq. (31) determines the flight-path angle as a function of velocity for most non-skipping entry trajectories.[16]

Comparing Fig. 2b and c with Fig. 4, the value of the flight-path angle near peak acceleration appears to be a better representation of the constant flight-path angle γ^* than the initial flight-path angle. The velocity at this condition, $V^* = V_{a_{max}}$, can be found using existing relationships in the Allen-Eggers solution; V^* may then be used in Eq. 31 to determine γ^*. Either Allen-Eggers expression for $V_{a_{max}}$ may be used to determine V^*: Eq. (12) or the simplified expression, Eq. (25). Using the simplified expression for $V_{a_{max}}$ yields a more compact expression for γ^*. Substituting Eq. (25) into Eq. (31) gives:

$$\sin\gamma^* = \sin\gamma_0\,(2F - 1) \tag{33}$$

where

$$F = \left[1 + \frac{H}{R\tan^2\gamma_0}\left\{C\frac{V_C^2}{V_0^2} + \left(\frac{V_C^2}{V_0^2} - 1\right)\ln\left(1 - \frac{\beta\sin\gamma_0}{H\rho_0}\right)\right\}\right]^{1/2} \tag{33a}$$

and

$$C = \mathrm{Ei}(1) - \bar{\gamma} \approx 1.3179 \tag{33b}$$

The constant C need only be determined once to the desired accuracy. As such, this expression does not require repeated evaluation of the exponential integral.

Figure 4 shows the efficacy of the proposed method for estimating γ^* for the sample-return trajectory at different initial flight-path angles. The resulting values for γ^* more closely approximate numeric solutions of

flight-path angle as a function of velocity. The difference between the proposed method and using γ_0 for γ^* increases with more shallow initial flight-path angles, but improvement is present for all initial flight-path angles shown. Both options for computing V^* are shown; the additional complexity of using Eq. (12) with Eq. (31) does not yield results that are appreciably different from those generated by Eq. (33).

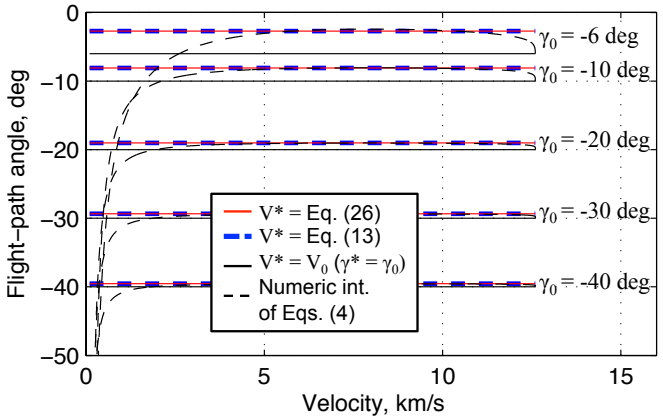

Figure 4. The proposed method for determining γ^* more closely approximates the flight-path angle as a function of velocity than setting $\gamma^* = \gamma^0$.

2. Improvements to Approximation Accuracy

The proposed method for determining γ^* improves the accuracy of the Allen-Eggers approximate solution across all three example cases (Fig. 5 and Fig. 6). The improvement is most significant for the sample-return example: deceleration and flight-path angle estimation error is reduced by nearly 40% near mid-trajectory. For the LEO-return case, error is reduced and more balanced about zero, but remains large. Improvements to the strategic case are small.

As shown in Fig. 6, estimates of vehicle states at peak acceleration and heat rate are improved for all three cases with the exception of the peak heat rate for the LEO-return case. This increase in error is accompanied by an equally large decrease in the error for the estimate of the peak deceleration, as well as smaller reductions in error for estimates of the velocity and altitude at these conditions.

B. Bounding the Domain of Applicability

Figure 7 shows the Allen-Eggers approximate altitude-velocity profile relative to the numeric solution to the equations of motion early and late in the trajectory as a function of the normalized velocity. Early in the trajectory (Fig. 7b), the Allen-Eggers approximation is invalid because vehicle dynamics are dominated by gravity, which is explicitly neglected. At high altitudes, atmospheric density is low, and therefore drag is low, and gravity dominates, causing the vehicle to accelerate as it descends into the planetary gravity well. As vehicle altitude decreases, atmospheric density builds, causing drag to increase and surpass gravity as the dominate force, causing the vehicle to decelerate. There is a point at which the drag and gravity forces are balanced: above this point, gravity dominates; below, drag dominates. The Allen-Eggers approximation becomes much more accurate once drag dominates the dynamics.

Late in the trajectory, the Allen-Eggers approximation error becomes large again (Fig. 7a). After passing through peak deceleration vehicle velocity continues to decrease, decreasing dynamic pressure and the drag force. Eventually, the drag force decreases enough that gravity becomes significant again, causing a negative flight-path angle rate known as the gravity turn. In this region of the trajectory, the Allen-Eggers assumptions on gravity and constant flight-path angle are both violated.

While the Allen-Eggers approximate solution shows significant error early and late in the example trajectory where its underlying assumptions are invalid, it is accurate for the middle of entry trajectories, encompassing the hypersonic regime. The direct link between the inaccuracies in the Allen-Eggers approximate solution early and late in the trajectory and the approximation's underlying assumptions suggest that a bounded domain can be identified, based on the equations of motion, over which the approximate solution is valid.

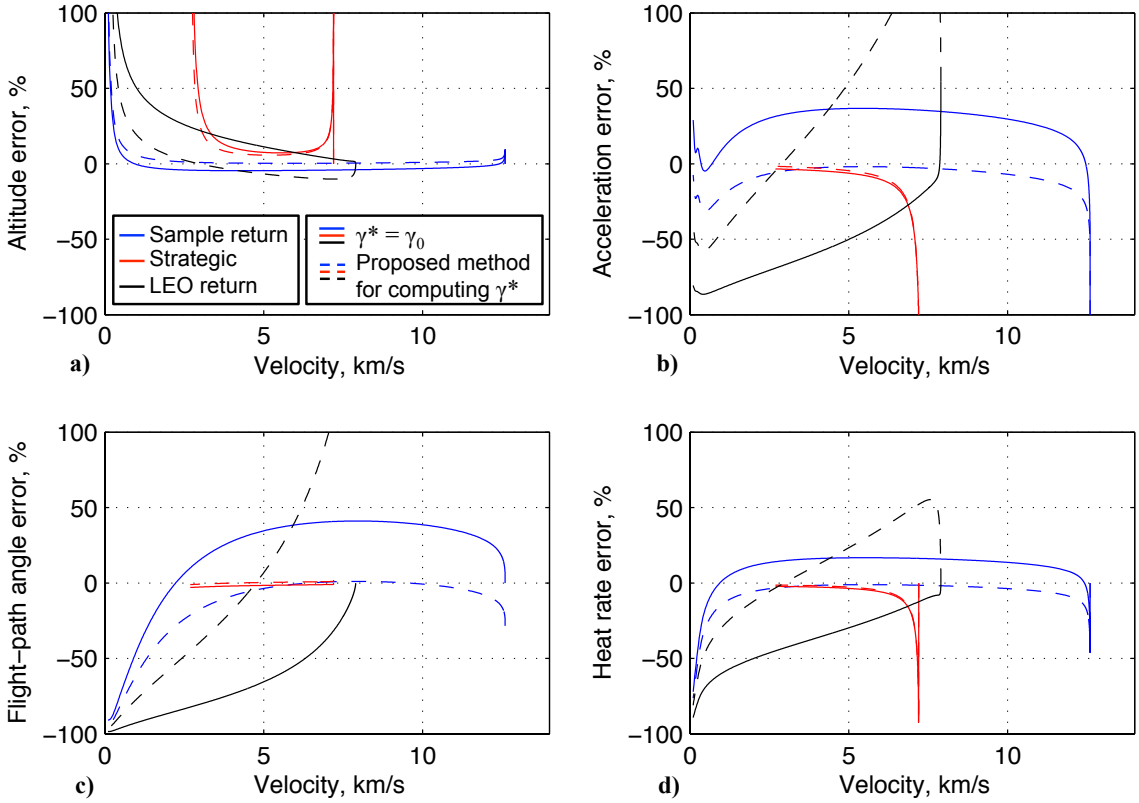

Figure 5. Approximation error with and without the proposed method for computing γ^*.

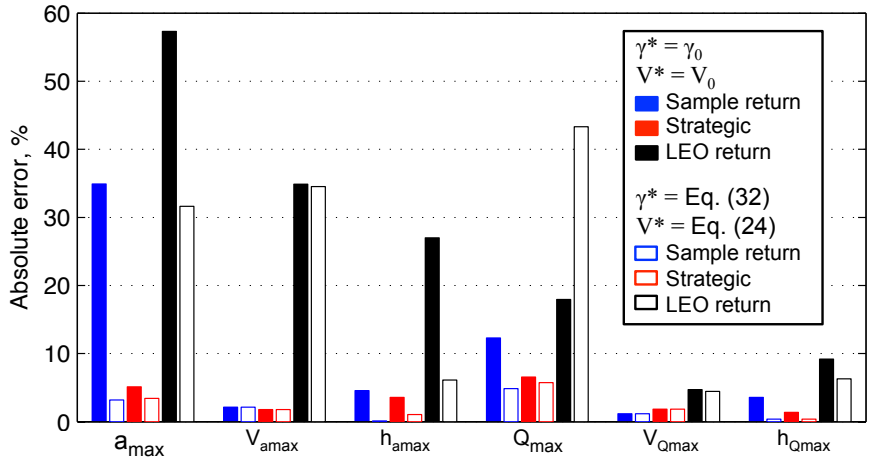

Figure 6. Vehicle states at peak conditions for $\gamma^* = \gamma_0$ and the proposed method of estimating γ^*.

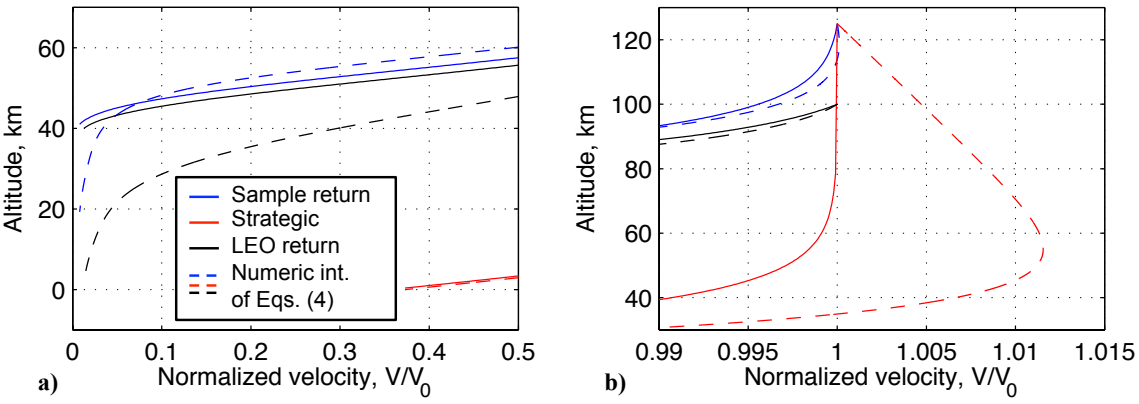

Figure 7. Allen-Eggers approximation error in altitude-velocity profile a) late and b) early in trajectory.

1. *Bound on Minimum Velocity*

A minimum-velocity bound on the domain of applicability for the Allen-Eggers approximate solution may be derived by considering Eq. (4b) for ballistic vehicles, rearranged:

$$\frac{d\gamma}{dt} = \left(\frac{V}{R+h} - \frac{g}{V}\right)\cos\gamma \tag{34}$$

As shown in Figs. 2c and 7a, the Allen-Eggers approximate solution becomes inaccurate when the flight-path angle begins to change significantly, indicating a nonzero (and negative) value of $d\gamma/dt$. Since $\cos\gamma$ tends to decrease with increasingly negative γ, any significant increase in the magnitude of $d\gamma/dt$ must be caused by an increase in the magnitude of the other factor. Since larger values of $d\gamma/dt$ occur late in the trajectory and the sign of $d\gamma/dt$ is negative, one can say that a significant $d\gamma/dt$ results when the gravity term, g/V, is larger than the range-rate term, $V/(R+h)$, by some factor, δ^2, and the Allen-Eggers approximation is only valid for velocities above that point:

$$\delta^2\left(\frac{g}{V}\right) > \frac{V}{R+h} \tag{35}$$

Neglecting h relative to R (a good assumption at low altitudes near the end of the trajectory) and solving for V determines a lower limit on velocity past which the gravity term exceeds the range-rate term by the factor δ^2:

$$V > \sqrt{\delta^2 gR} \tag{36}$$

Defining the minimum acceptable final velocity as V_f, rearranging, and designating δ as δ_V, one finds the minimum final velocity is:

$$V_f = \delta_V\sqrt{gR} = \delta_V V_C \tag{37}$$

This shows that V_f is merely a faction of the circular velocity, the velocity of a notional circular orbit at the planetary surface, and δ_V is a stand-off parameter that relates the lower bound of the Allen-Eggers velocity domain to planetary parameters. Figure 8 shows the minimum velocity for three values of δ_V. Larger values of δ_V imply a more restrictive domain for the Allen-Eggers approximation.

An appropriate value of δ_V may be chosen by examining the Allen-Eggers approximation error as a function of δ_V, as shown in Fig. 9a for the sample-return example trajectory. The figure indicates that a δ_V of 0.05 will limit approximation error in altitude, deceleration, and heat rate to less than approximately 20%. While the flight-path angle error remains large at this value of δ_V, the Allen-Eggers solution does not attempt to estimate the flight-path angle, making this error less significant.

2. *Bound on Initial Dynamic Pressure*

A bound on the initial state may also be derived to complete the specification of the domain of applicability for the Allen-Eggers approximation. Figure 7b shows that the Allen-Eggers approximation is inaccurate in

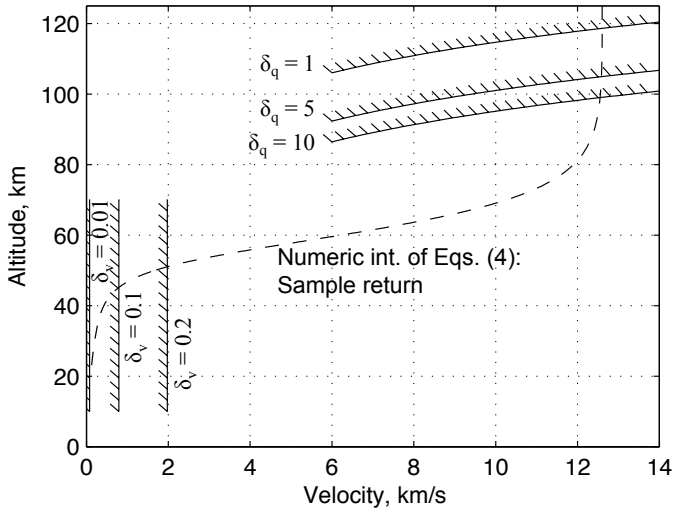

Figure 8. Example bounds on the Allen-Eggers domain of applicability for the sample-return example case for several values of δ_V and δ_q.

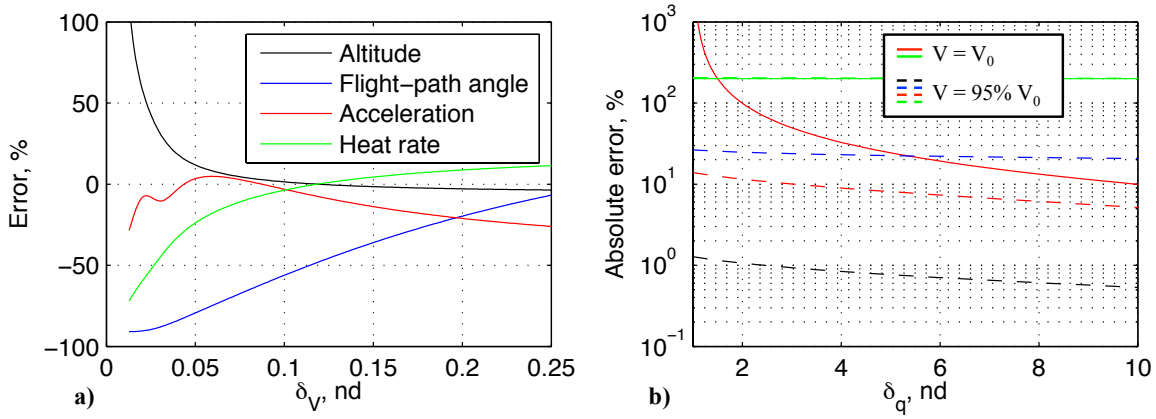

Figure 9. Allen-Eggers approximation error versus a) the final velocity stand-off factor δ_V and b) the initial dynamic pressure stand-off factor δ_q.

the region when velocity is increasing under the influence of gravity. The point at which the gravity and drag forces balance occurs when velocity is at a maximum. At this point, from Eq. (4a):

$$\frac{dV}{dt} = 0 = -\frac{\rho}{2\beta}V^2 - g\sin\gamma \tag{38}$$

The Allen-Eggers approximation assumes the gravity force is negligible relative to the drag force, or:

$$\frac{\rho}{2\beta}V^2 \gg -g\sin\gamma \tag{39}$$

where $\gamma < 0$ for entry, making the right-hand side positive. Rearranging:

$$q \gg -g\beta\sin\gamma \tag{40}$$

The limit on the initial dynamic pressure, q_0, may then be defined in terms of a standoff factor, δ_q, and the initial flight-path angle such that:

$$q_0 = -\delta_q g\beta\sin\gamma_0 \tag{41}$$

Eq. (41) defines a limit on the initial dynamic pressure, and therefore on the acceptable set of (V_0, h_0), as a function of the initial flight-path angle, vehicle properties, planetary properties, and the stand-off factor δ_q. A δ_q value of 1 indicates the dynamic pressure at maximum velocity. Figure 8 shows how this dynamic pressure limit leads to limits on the initial velocity and altitude for several values of δ_q. Conventionally, the initial conditions for entry are defined at an arbitrary altitude; Eq. (41) defines initial conditions for entry trajectories based on when the atmosphere begins to dominate vehicle dynamics.

Similarly to δ_V, an appropriate value for δ_q may be chosen by examining the Allen-Eggers state approximation error as a function of δ_q. Figure 9b shows approximation error for sample-return trajectory at V_0 and at 95% of V_0 as a function of δ_q. States at two velocities are shown because there is no approximation error in the altitude or flight-path angle at the initial state. Heat rate percent error is large at both points, but the magnitude of this error is small due to the high altitude and low density. A δ_q value of 2 is chosen to provide margin relative to the maximum velocity point ($\delta_q = 1$) while limiting the initial approximation error in acceleration to 100%.

3. Improvements to Approximation Accuracy

Figures 10 and 11 show the decrease in approximation error for the example trajectories with the Allen-Eggers approximation restricted to its domain of applicability by limits on V_f and q_0 with $\delta_V = 0.05$ and $\delta_q = 2$. Modest improvement in approximation error is apparent for the sample-return and strategic cases. No improvement is seen in the LEO-return case because its initial dynamic pressure exceeds that associated with a δ_q of 2.

C. Closed-Form Expressions for Range

Closed-form, explicit approximations for entry range have generally been restricted to vehicles with nonzero L/D, such as equilibrium glide[20] and Sänger's steep lifting entry.[1] For ballistic entry, approximate trajectory solutions in the literature either omit range, evaluate range through integrals that must be solved numerically,[21] or utilize highly-truncated series approximations.[22] No closed-form analytic expression for ballistic entry range has been identified in the current literature. Analytic solutions to the states of the equations of motion are often complex and must be combined into an additional integral to compute range. The complexity of this range integrand typically defies analytic solution.

Modern computational symbolic integration has been used to develop closed-form expressions for range and range to go as functions of velocity for the Allen-Eggers approximate solution. These range expressions extend the Allen-Eggers approximate solution to cover all four states in Eqs. (4).

1. Derivation

The energy over weight for an entry vehicle is defined by:

$$E = \frac{1}{mg}\left(\frac{1}{2}mV^2 + mgh\right) = \frac{V^2}{2g} + h \tag{42}$$

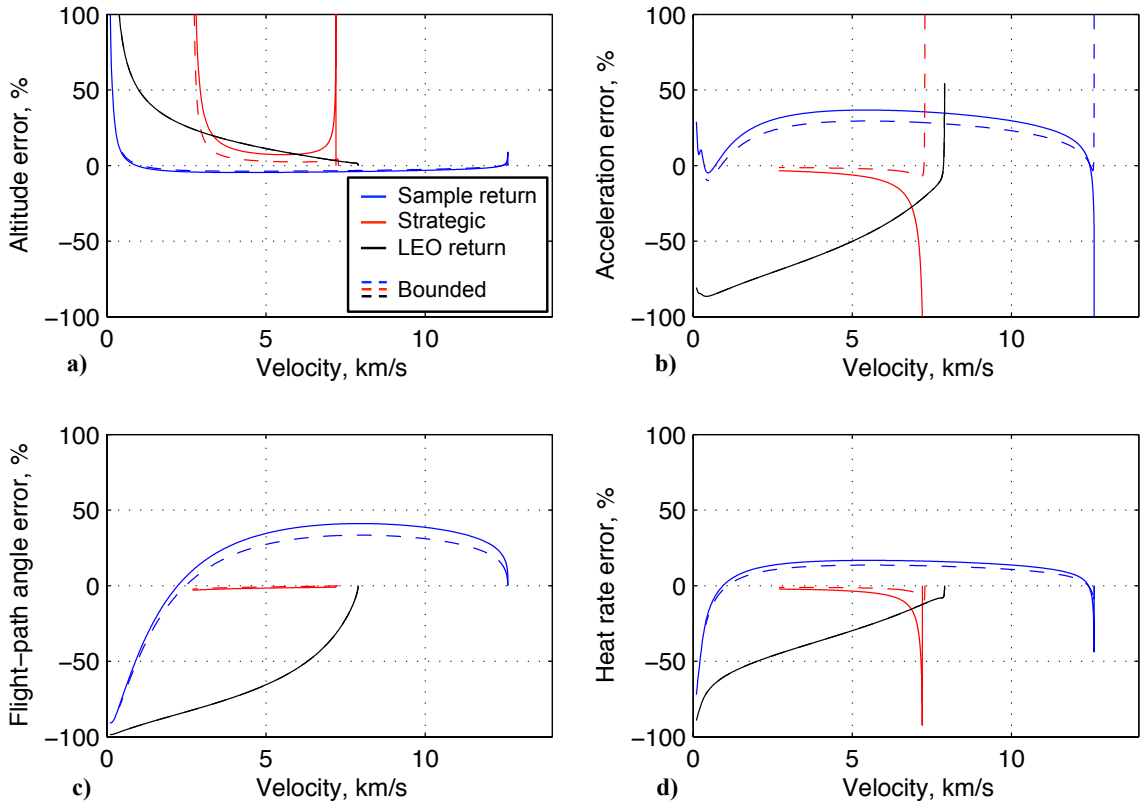

Figure 10. Approximation error for bounded and unbounded domains.

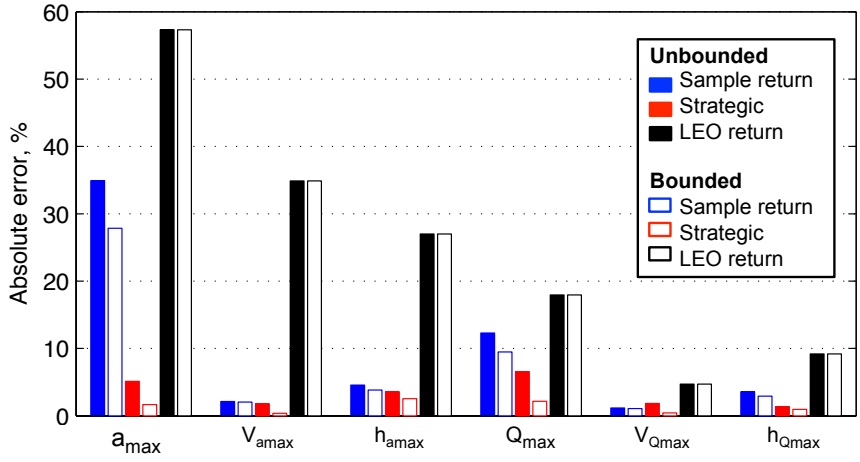

Figure 11. Allen-Eggers approximation error of vehicle states at peak conditions for bounded and unbounded domains.

The derivative of the energy over weight with respect to time is given by, substituting in Eqs. (4a) and (4c):

$$\frac{dE}{dt} = \frac{V}{g}\frac{dV}{dt} + \frac{dh}{dt} = -\frac{\rho}{2g\beta}V^3 \tag{43}$$

The derivative of the subtended range angle with respect to the energy over weight is then:

$$\frac{d\theta}{dE} = \frac{d\theta/dt}{dE/dt} = \frac{-2\beta g\cos\gamma}{\rho V^2(R+h)} \tag{44}$$

Define the range to be the distance traveled over the surface of a spherical planet, as shown in Fig. 12. Assuming the initial range S_0 and range angle θ_0 are zero, the range is related to the range angle by the arc-length formula for a spherical planet:

$$S = R\theta = R\int_{E_0}^{E} \frac{-2\beta g\cos\gamma}{\rho V^2(R+h)}dE \tag{45}$$

If the final range is S_f, the range to go is:

$$S_{togo} = S_f - S = R\int_{E}^{E_f} \frac{-2\beta g\cos\gamma}{\rho V^2(R+h)}dE \tag{46}$$

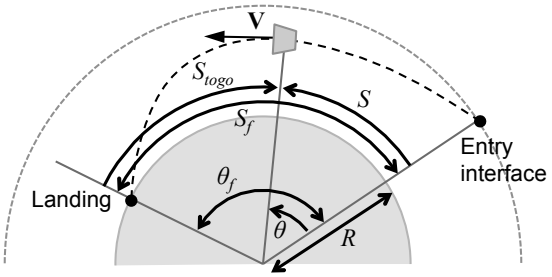

Figure 12. Planetary entry range and range angle.

A differential change in energy over weight can be described by:

$$dE = \frac{1}{2g}d(V^2) + dh \tag{47}$$

Applying Eq. (47) to Eq. (45), flipping integration limits to eliminate negative signs, and pulling constants outside the integrals, one finds:

$$S = \int_{V^2}^{V_0^2} \frac{R\beta\cos\gamma}{(R+h)\rho V^2}d(V^2) + \int_{h}^{h_0} \frac{2R\beta g\cos\gamma}{(R+h)\rho V^2}dh \tag{48}$$

This integral expression for range makes no assumptions relative to Eqs. (4) and has no analytic solution. Analytic solution is possible using the Allen-Eggers assumptions: neglecting gravity eliminates the altitude integral and assuming a constant flight-path angle simplifies the velocity integral. Also, using Eq. (9):

$$\rho = \frac{\beta\sin\gamma^*}{H}\ln\left(\frac{V^2}{V_1^2}\right) + \rho_1 \tag{49a}$$

$$h = h_{ref} - H\ln\left[\frac{\beta\sin\gamma^*}{\rho_{ref}H}\ln\left(\frac{V^2}{V_1^2}\right) + \frac{\rho_1}{\rho_{ref}}\right] \tag{49b}$$

Applying these assumptions, substituting Eqs. (49) for altitude and density, and integrating from state 2 to the initial state, with state 1 as a reference state:

$$S_2 = R\beta\cos\gamma^*\int_{V_2^2}^{V_0^2}\left\{\left[R + h_{ref} - H\ln\left(\frac{\beta\sin\gamma^*}{\rho_{ref}H}\ln\left(\frac{(V^2)}{V_1^2}\right) + \frac{\rho_1}{\rho_{ref}}\right)\right]\times \left[\frac{\beta\sin\gamma}{H}\ln\left(\frac{(V^2)}{V_1^2}\right) + \rho_1\right](V^2)\right\}^{-1} d(V^2) \tag{50}$$

Evaluating this integral analytically results in a closed-form solution for range as a function of velocity:

$$S_2 = R\cot\gamma^*\left(\ln\left\{H\ln\left[\frac{\rho_1}{\rho_{ref}}+\frac{\beta\sin\gamma^*}{H\rho_{ref}}\ln\left(\frac{V_2^2}{V_1^2}\right)\right]-h_{ref}-R\right\}-\right.$$
$$\left.\ln\left[H\ln\left(\frac{\rho_1}{\rho_{ref}}+\frac{\beta\sin\gamma^*}{H\rho_{ref}}\ln\left(\frac{V_0^2}{V_1^2}\right)\right)-h_{ref}-R\right]\right) \quad (51)$$

Similarly, starting from Eq. (46), the range to go at a particular velocity is given by:

$$S_{2,togo} = R\cot\gamma^*\left(\ln\left\{H\ln\left[\frac{\rho_1}{\rho_{ref}}+\frac{\beta\sin\gamma^*}{H\rho_{ref}}\ln\left(\frac{V_f^2}{V_1^2}\right)\right]-h_{ref}-R\right\}-\right.$$
$$\left.\ln\left[H\ln\left(\frac{\rho_1}{\rho_{ref}}+\frac{\beta\sin\gamma^*}{H\rho_{ref}}\ln\left(\frac{V_2^2}{V_1^2}\right)\right)-h_{ref}-R\right]\right) \quad (52)$$

Alternately, solving Eq. (50) assuming $R/(R+h) \approx 1$ and setting $V_1 = V_0$, the range may be reduced to a simple function of altitude:

$$S_2 = \cot\gamma^*\left(h_2 - h_0\right) \quad (53)$$

Eqs. (51) to (53) are closed-form, analytic expressions for range as a function of velocity or altitude, vehicle and planetary parameters, initial conditions, and the Allen-Eggers constant flight-path angle. The additional assumptions made in deriving Eq. (53) make the trajectory is a straight line; this is not the case for Eqs. (51) and (52).

2. Example Application

Figure 13 shows Eqs. (51) and (52) applied to the example trajectories. The approximation is applied over the domain bounded by δ_V and δ_q values of 0.05 and 2, respectively, and γ^* is determined using Eq. (33). Figure 13a uses the Allen-Eggers equations for the vehicle state at peak acceleration for the 1 reference point; Fig. 13b uses the initial condition for the 1 reference point. Range and range-to-go estimates in Fig. 13a and b are good for the strategic case; estimation of range to go appears to result in lower error relative to range for all three cases.

Figure 14 shows the percent and absolute approximation errors for Eq. (51). Initial range predictions have near-zero error because the initial range traveled is zero. For all three cases, the error quickly climbs to a near-constant value: about 10% for the sample-return case, -2% for the strategic case, and -50% for the LEO-return case. While approximation error is low for the strategic case, the 10% error for the sample-return case corresponds to an absolute error of nearly 80 km.

Approximation error for range to go (Eq. (52)) is shown in Fig. 15. Percent error is within 2% for the sample-return case and less than 1% for the strategic case. Approximation error is below 3% for even the LEO-return case. Overall, errors are approximately an order of magnitude less than they are for the range estimate. In addition, because range to go is always decreasing, the absolute error trends to a near-zero final value.

These results indicate that while the range equation provides a good first-order estimate of the range traveled during entry, the range-to-go equation accuracy may be good enough for onboard guidance and targeting. This result is especially significant for drag-modulation trajectory control for ballistic entry.[23]

D. Trajectory States as a Function of Time

The Allen-Eggers approximate solution makes three significant assumptions relative to the planar equations of motion (as given in Eqs. (4)):

1. Ballistic entry: $L/D = 0$
2. Constant flight-path angle: $d\gamma/dt = 0$
3. Gravity is negligible relative to drag: $\rho V^2/(2\beta) \gg -g\sin\gamma$

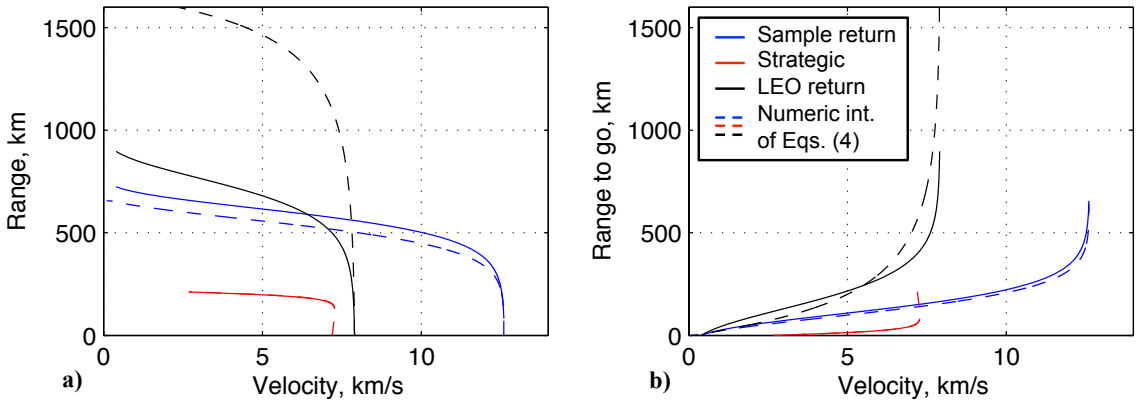

Figure 13. Estimates of a) range and b) range to go.

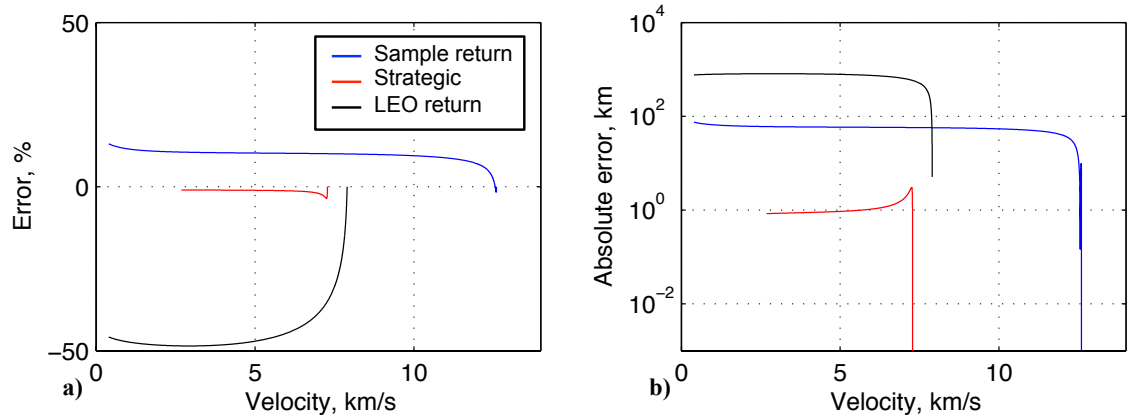

Figure 14. Range estimation error: a) percent error with respect to total range and b) absolute error.

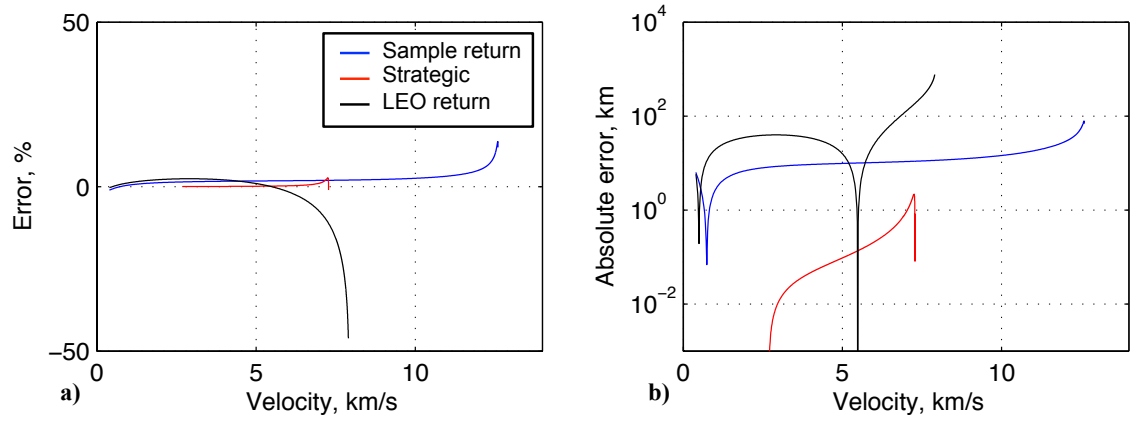

Figure 15. Range-to-go estimation error: a) percent error with respect to total range and b) absolute error.

The equations of motion with the above assumptions applied are, reduced from Eqs. (4):

$$\frac{dV}{dt} = -\frac{\rho_{ref}}{2\beta} \exp\left(\frac{h_{ref} - h}{H}\right) V^2 \tag{54a}$$

$$\frac{d\gamma}{dt} = 0 \tag{54b}$$

$$\frac{dh}{dt} = V \sin\gamma^* \tag{54c}$$

$$\frac{d\theta}{dt} = \frac{V \cos\gamma^*}{R + h} \tag{54d}$$

The original Allen-Eggers approximate solution is an exact solution to these reduced equations when t is eliminated by combining Eq. (54a) and (54c).

However, Eqs. (54) can be integrated directly with respect to time, yielding the result:

$$V = C_1 \exp\left[\frac{\rho_{ref} H}{2\beta \sin\gamma^*} \exp\left(\frac{h_{ref} - h}{H}\right)\right] \tag{55a}$$

$$\gamma = \gamma^* \tag{55b}$$

$$-H\mathrm{Ei}\left[-\frac{\rho_{ref} H}{2\beta \sin\gamma^*} \exp\left(\frac{h_{ref} - h}{H}\right)\right] = C_1 \sin\gamma^* t + C_2 \tag{55c}$$

$$\theta = C_3 + \cot\gamma^* \ln(R + h) \tag{55d}$$

If the initial condition is given by V_0, h_0, $\gamma_0 = \gamma^*$, $\theta_0 = 0$, and $t_0 = 0$, the constants of integration are:

$$C_1 = V_0 \exp\left[-\frac{\rho_{ref} H}{2\beta \sin\gamma^*} \exp\left(\frac{h_{ref} - h_0}{H}\right)\right] \tag{56a}$$

$$C_2 = -H\mathrm{Ei}\left[-\frac{\rho_{ref} H}{2\beta \sin\gamma^*} \exp\left(\frac{h_{ref} - h_0}{H}\right)\right] \tag{56b}$$

$$C_3 = -\cot\gamma^* \ln(R + h_0) \tag{56c}$$

Eq. (55a) is similar in structure to the altitude-velocity profile first derived by Allen and Eggers, and is exactly that derived earlier (Eq. (9)) when the value for C_1 (Eq. (56a)) is applied. The range equations, Eqs. (51) and (52), may be derived from Eq. (55d) by multiplying by R to convert from range angle to range and replacing instances of h with V using Eq. (9). Lastly, Eq. (55c) provides a relationship between time and altitude.

Evaluation of Eqs. (55) is most convenient when altitude is chosen for the domain; this allows time to be found without iterative root finding. The vehicle states are shown as a function of time in Fig. 16; acceleration and heating as a function of time are shown in Fig. 17. Eqs. (55) show good agreement with Eqs. (4) for the strategic case. Agreement for the sample-return case is good for approximately 100 s, which encompasses the acceleration and heat-rate pulses. Agreement for the LEO-return case is poor as in previous examples.

Numerical difficulties may occur when evaluating Eqs. (55) due to the exponential integral in Eq. (55c): for large arguments (greater than 100), the exponential integral is very large, i.e. hundreds of orders of magnitude greater than its argument. These large arguments occur at low altitudes for small β and shallow γ^* and correspond to violations of two Allen-Eggers assumptions. First, shallow trajectories (shallow γ^*) are not well-approximated by a constant flight-path angle, as shown by the LEO-return example throughout this study. Second, low-β vehicles decelerate higher in the atmosphere. While small β increases the magnitude of the drag force relative to gravity (see Eq. (4a), it also causes gravity to become significant at higher altitudes, violating the Allen-Eggers negation of gravity. Figure 16c shows an example of this for the sample-return trajectory: the Allen-Eggers time history is a good approximation until an altitude of approximately 50 km, at which point the argument of the exponential integral on the left-hand side of Eq. (55c) becomes large causing the left-hand side of the equation to become very large, ultimately resulting in large, incorrect values of t.

Overall, the proposed solution for time during entry appears to offer benefits relative to Kumagai's expression for time of flight for ballistic entry.[24] Kumagai's solution requires the use of two series approximations,

one of which requires retention of at least seven terms to obtain satisfactory accuracy. The solution proposed in this study may be solved explicitly with appropriate selection of a domain and is directly related to the Allen-Eggers solution.

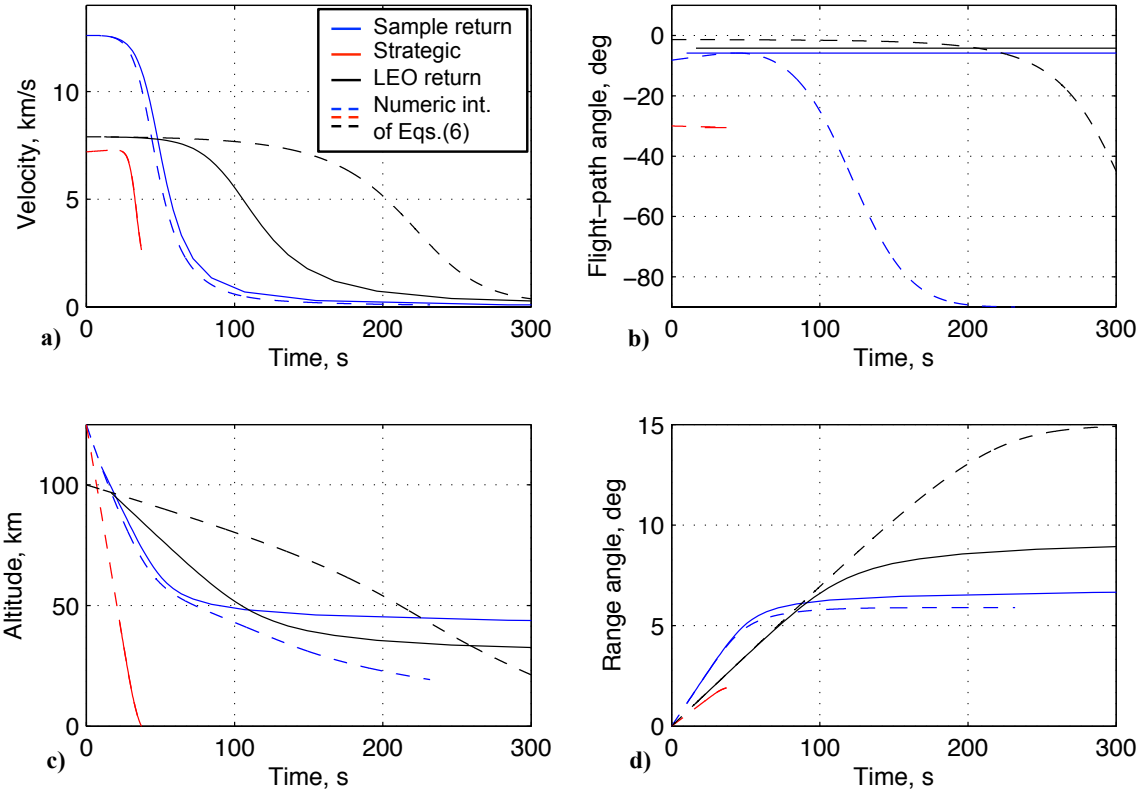

Figure 16. Comparison of states from the time-dependent Allen-Eggers solution with the two-degree-of-freedom equations of motion: a) velocity, b) altitude, c) flight-path angle, and d) range angle versus time.

V. Assessment of Approximation Error and Applicability

A. The Extended and Enhanced Allen-Eggers Approximation

Figure 18 shows example applications of the extended and enhanced Allen-Eggers approximation. Application of the original Allen-Eggers approximation from Fig. 2 is shown in grey. Figure 19 shows the approximation error of the original and extended and enhanced versions. Results show that significant improvements in approximation error relative to the two-degree-of-freedom equations of motion were achieved. Approximation error for the strategic case is below 5% across Fig. 19, with the exception of altitude at low velocities (Fig. 19a); this spike in error is due to numerical error computation near zero altitude. Approximation error for the sample-return example is below 10% over most of the hypersonic flight regime, typically the most important part of an entry trajectory. The LEO-return example exhibits large, but reduced and more balanced error. This is not unexpected, as the initial flight-path angle for this example is too shallow for the Allen-Eggers negation of gravity to be a good assumption.

Figure 20 shows the approximation error in peak conditions for the extended and enhanced solution relative to the original. Significant improvement is apparent across nearly all parameters, with the exception of the peak heat rate estimate for the LEO-return case.

B. Applicability to Other Initial Conditions

Initial velocity and flight-path angle were varied for the vehicles from the three examples used in this study to determine the applicability of the Allen-Eggers approximate solution across a broader mission set. Domains

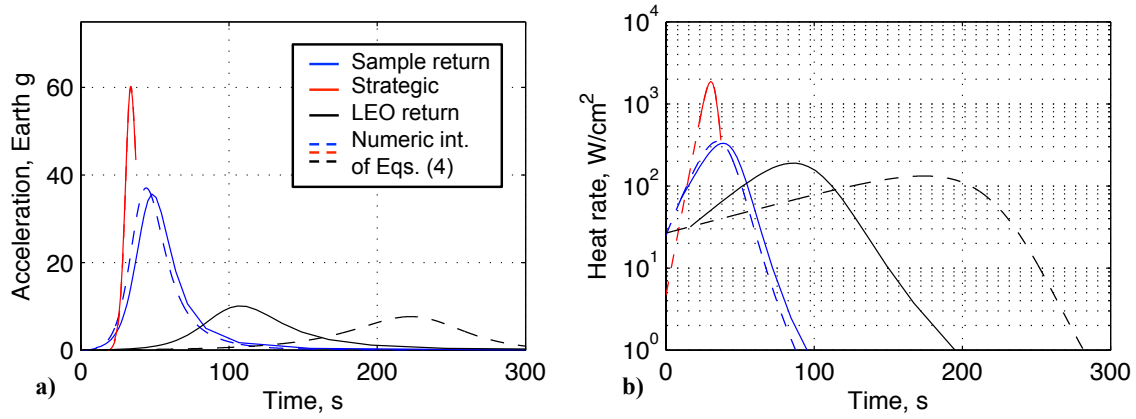

Figure 17. Comparison of states from the time-dependent Allen-Eggers solution with the two-degree-of-freedom equations of motion: a) acceleration and b) heat rate versus time.

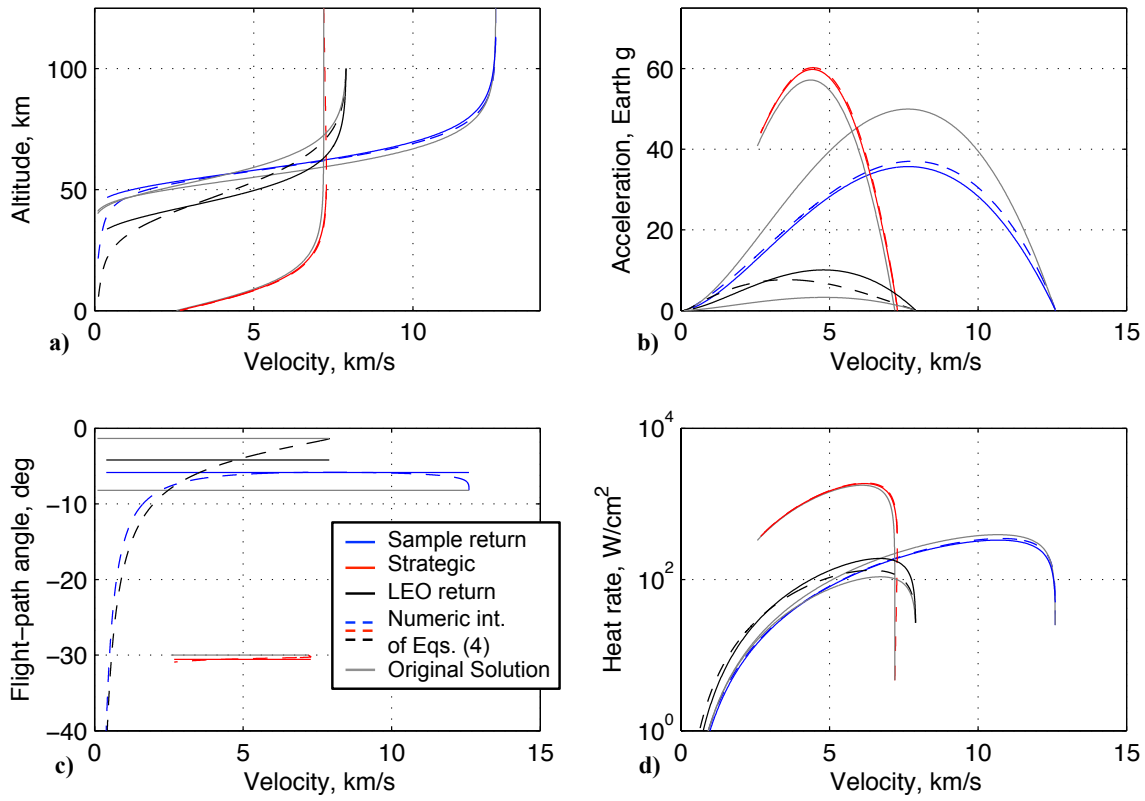

Figure 18. Example application of the extended and enhanced Allen-Eggers approximate solution.

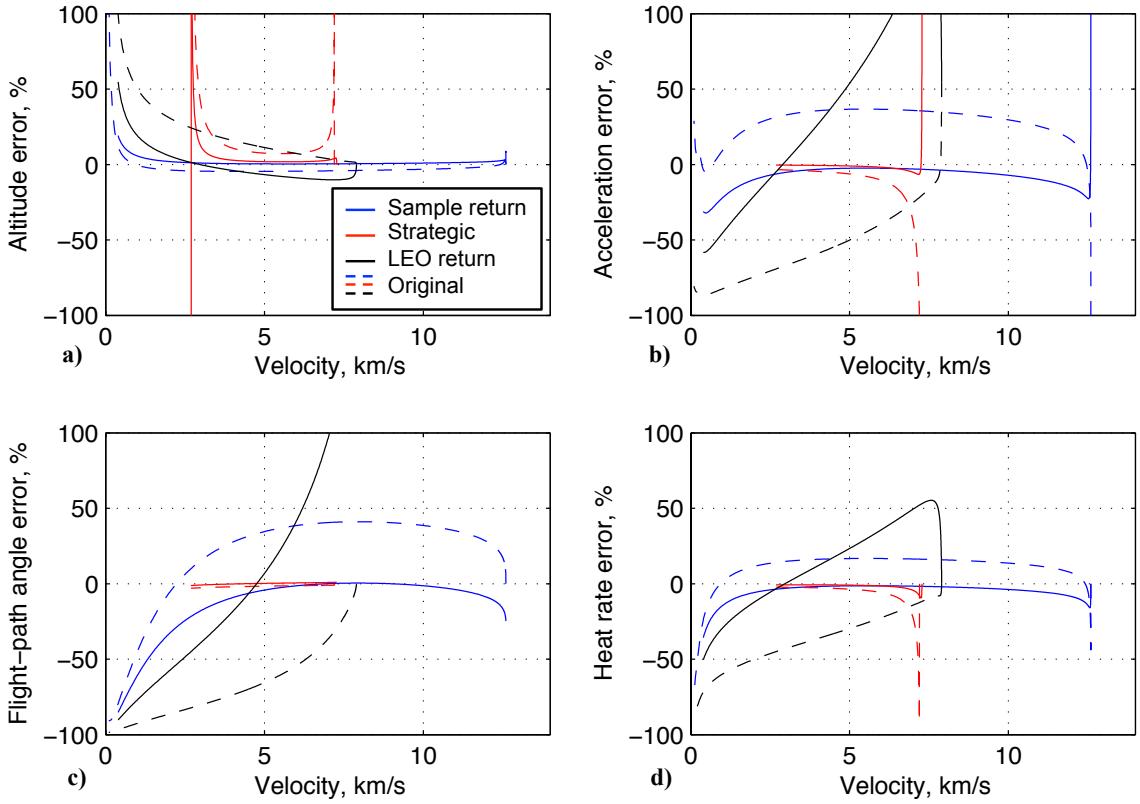

Figure 19. Approximation error for the original and extended and enhanced Allen-Eggers approximate solutions.

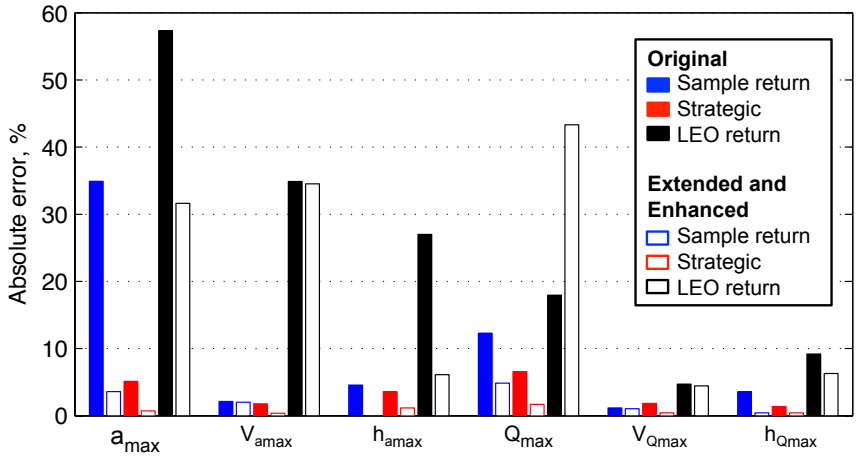

Figure 20. Approximation error for the original and extended and enhanced Allen-Eggers approximate solutions.

for individual trajectories were bound by δ_V and δ_q values of 0.05 and 2, respectively.

Contours of the integrated trajectory approximation error (see Eq. (5)), normalized by the integrated error of each example, is shown for acceleration (Fig. 21), heat rate (Fig. 22), and range (Fig. 23). These figures all indicate that the Allen-Eggers approximation error is lower for faster, steeper entry trajectories, as one would expect given the Allen-Eggers assumptions. More interestingly, approximation error is on the order of that of the sample-return case in Fig. 18 for trajectories with initial flight-path angles steeper than -7 deg at high initial velocities and steeper than -3 deg for low velocities. As one might expect, the LEO-return example falls outside this region of low approximation error.

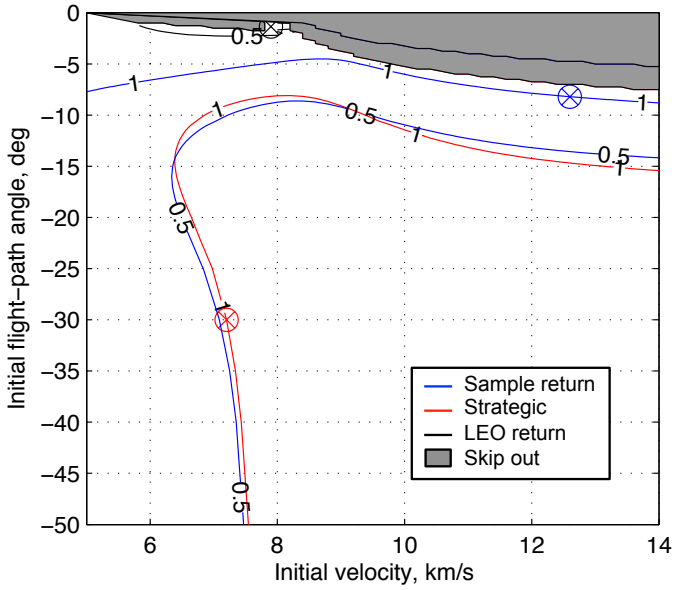

Figure 21. Normalized integrated error for acceleration with respect to velocity.

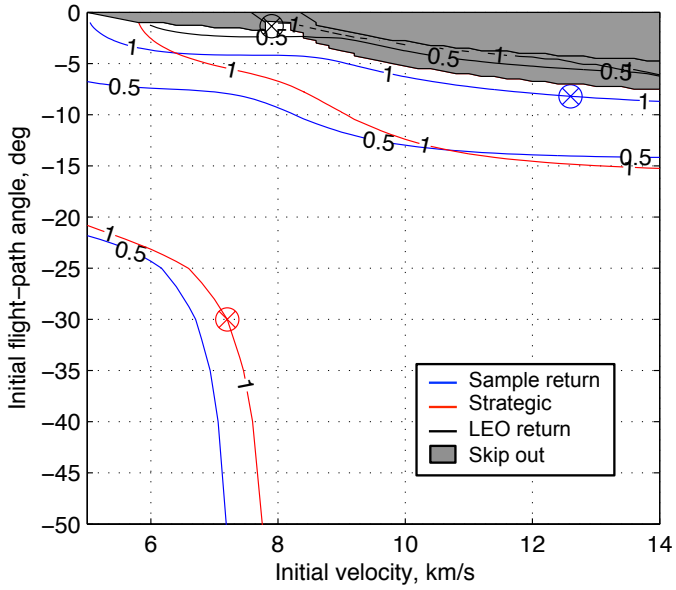

Figure 22. Normalized integrated error for heat rate with respect to velocity.

Figure 24 shows the absolute percent error in the Allen-Eggers approximation of peak acceleration and heat rate. Similar to the integrated error, approximation error is lowest for steep, fast entry trajectories. However, approximation errors within 1% are possible for most trajectories; nearly the entire range of initial

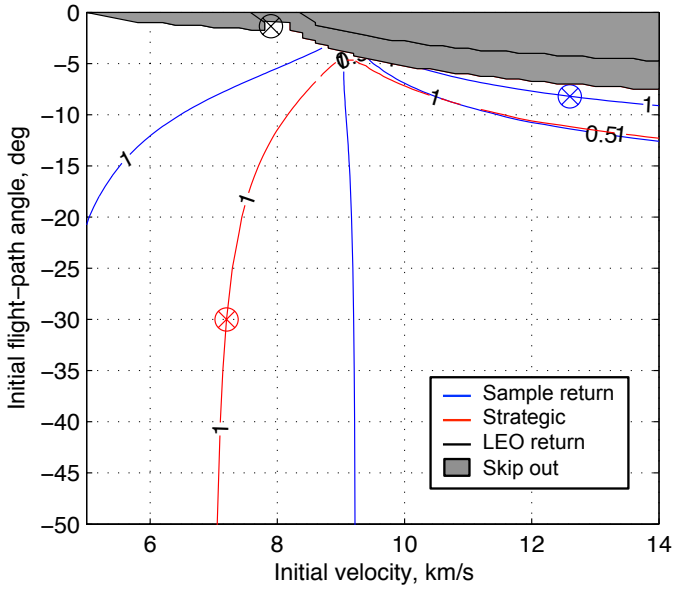

Figure 23. Normalized integrated error for range with respect to velocity.

conditions studied shows approximation error less than 5%.

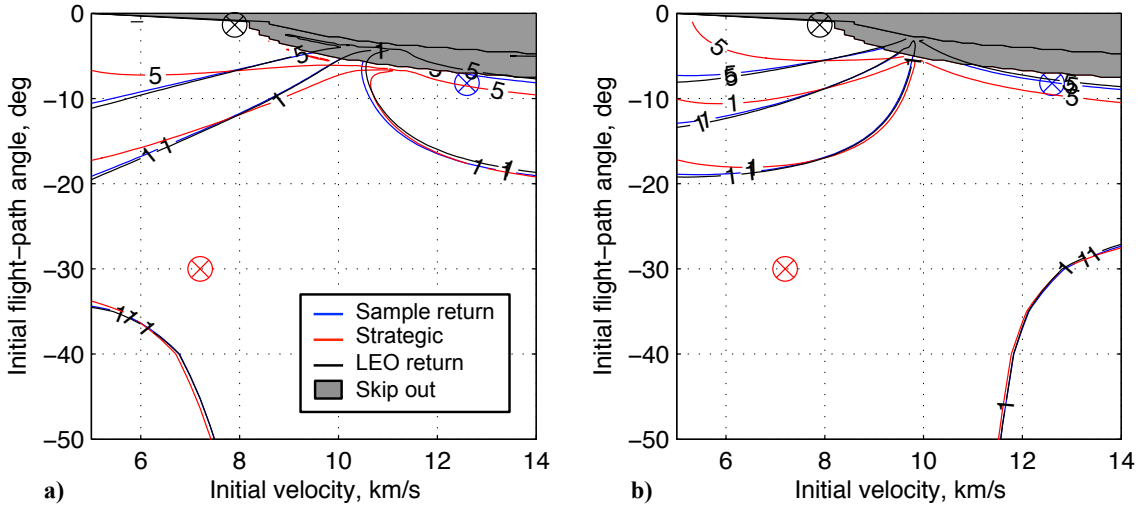

Figure 24. Absolute percent error for a) peak acceleration and b) peak heat rate.

VI. Conclusions

The Allen-Eggers approximate solution to the equations of motion for ballistic entry has been extended and enhanced. A method has been developed for determining appropriate values for the constant flight-path angle assumed to exist in the Allen-Eggers approximate solution. Determining the constant flight-path angle for use in the Allen-Eggers solution has long been viewed as a practical challenge when applying the approximation to a real-world problem. The proposed method preserves the simplicity and speed inherent in the Allen-Eggers approximation. The domain of applicability for the approximation has been bounded by nondimensional stand-off factors for the final velocity and initial dynamic pressure. Appropriate values for these factors ensure that approximation errors associated with the Allen-Eggers solution are limited to acceptable magnitudes. Closed-form, analytic expressions for range and time have been developed, extending the Allen-Eggers approximation to all four two-dimensional vehicle states and allowing estimation of the time of flight for ballistic entry vehicles. The error present in the range-to-go expression is particularly low, making it a candidate for onboard guidance and targeting applications.

These enhancements and extensions address key weaknesses in the original solution and a gap in the current literature: existing analytic solutions for ballistic entry do not provide closed-form expressions for range. When combined, these extensions and enhancements improve the accuracy of the Allen-Eggers approximate solution by an order of magnitude in some cases. Results show that the extended and enhanced Allen-Eggers solution provides good accuracy across a range of ballistic coefficients and is applicable for ballistic entries at Earth with initial flight-path angles steeper than -7 deg.

Acknowledgement

This work was supported by a NASA Space Technology Research Fellowship.

References

[1]Sänger, E. and Bredt, J., "A Rocket Drive for Long Range Bombers," Aug. 1944, translated by M. Hamermesh, Navy Department CGD-32.

[2]Allen, H. J. and Eggers, A. J., "A Study of the Motion and Aerodynamic Heating of Ballistic Missiles Entering the Earth's Atmosphere at High Supersonic Speeds," NACA-TR-1381, 1958.

[3]Chapman, D. R., "An Approximate Analytical Method for Studying Entry Into Planetary Atmospheres," NASA R-11, 1959.

[4]Loh, W. H. T., "A Second-Order Theory of Entry Mechanics Into a Planetary Atmosphere," *Journal of Aerospace Sciences*, Vol. 29, No. 10, 1962, pp. 1210–1221.
doi: 10.2514/8.9761

[5]Vinh, N. X., Busemann, A., and Culp, R. D., *Hypersonic and Planetary Entry Flight Mechanics*, University of Michigan Press, Ann Arbor, MI, 1980.

[6]Ceruzzi, P. E., *Beyond the Limits: Flight Enters the Computer Age*, MIT Press, Cambridge, MA, 1989.

[7]Allen, H. J. and Eggers, A. J., "A Study of the Motion and Aerodynamic Heating of Missiles Entering the Earth's Atmosphere at High Supersonic Speeds," NACA RM-A53D28, Aug. 1953.

[8]Regan, F. J. and Anandakrishnan, Satya M., *Dynamics of Atmospheric Re-Entry*, American Institute of Aeronautics and Astronautics, Reston, VA, 1993, pp. 179–184.

[9]Anderson, J. D., *Hypersonic and High Temperature Gas Dynamics*, American Institute of Aeronautics and Astronautics, Reston, VA, 2000.

[10]Desai, P. N. and Qualls, G. D., "Stardust Entry Reconstruction," *Journal of Spacecraft and Rockets*, Vol. 47, No. 5, Sep. 2010, pp. 736–740.
doi:

[11]King, H. H., "Ballistic Missile Re-Entry Dispersion," *Journal of Spacecraft and Rockets*, Vol. 17, No. 3, May 1980, pp. 240–247.
doi: 10.2514/3.28031

[12]Kontinos, D. A. and Wright, M. J., "Introduction: Atmospheric Entry of the Stardust Sample Return Capsule," *Journal of Spacecraft and Rockets*, Vol. 47, No. 6, Nov. 2010, pp. 865–867.
doi: 10.2514/1.52887

[13]Oberg, J., "Internal NASA Document Gives Clues to Scary Soyuz Return Flight," *IEEE Spectrum* (online), 1 May 2008, URL: http://spectrum.ieee.org/aerospace/space-flight/internal-nasa-documents-give-clues-to-scary-soyuz-return-flight [cited 20 May 2014].

[14]Hoff, N. J., "Harry Julian Allen," *Memorial Tributes*, Vol. 1, National Academy of Engineering, Washington, DC, 1979.

[15]Sutton, K. and Graves, R. A., "A General Stagnation-point Convective-heating Equation for Arbitrary Gas Mixtures," NASA TR R-376, November 1971.

[16]Citron, S. J. and Meir, T. C., "An Analytic Solution for Entry Into Planetary Atmospheres," *AIAA Journal*, Vol. 3, No. 3, Mar. 1965, pp. 470–475.
doi: 10.2514/3.2888

[17]Yaroshevskiy, V. A., "Approximate Calculation of Trajectory for Entry Into Atmosphere I," *Kosmicheskiye Issledovaniya* (Cosmic Research), Vol. 2, No. 4, 1964, translated by USAF Foreign Technology Division, AD 605513.

[18]Yaroshevskiy, V. A., "Approximate Calculation of Trajectory for Entry Into Atmosphere II," *Kosmicheskiye Issledovaniya* (Cosmic Research), Vol. 2, No. 5, 1964, translated by USAF Foreign Technology Division, AD 608083.

[19]Cody, W. J. and Thacher, H. C., "Rational Chebyshev Approximations for the Exponential Integral $E_1(x)$," *Mathematics of Computation*, Vol. 22, No. 103, Jul. 1968, pp. 641–649.

[20]Hale, F. J., *Introduction to Space Flight*, Prentice-Hall, Englewood Cliffs, NJ, 1994.

[21]Moe, M. M., "An Approximation to the Re-Entry Trajectory," *ARS Journal*, Vol. 30, No. 1, Jan. 1960, pp. 50–53.
doi: 10.2514/8.4984

[22]Kornreich, T. R., "Approximate Solutions for the Range of a Nonlifting Re-Entry Trajectory," *AIAA Journal*, Vol. 1, No. 8, Aug. 1963, pp. 1925-1926.
doi: 10.2514/3.1960

[23]Putnam, Z. R. and Braun, R. D., "Precision Landing at Mars Using Discrete-Event Drag Modulation," *Journal of Spacecraft and Rockets*, Vol. 51, No. 1, Feb. 2014, pp. 128–138.
doi: 10.2514/1.A32633

[24]Kumagai, T. T., "Approximation of Time of Ballistic Entry," *Journal of Spacecraft and Rockets*, Vol. 1, No. 6, Nov. 1964, pp. 675–676.
doi: 10.2514/3.27721